SCEC Project #21035: Time-series InSAR analysis using ARIA standardized InSAR products in support of the Community Geodetic Model

Final Report

Gareth Funning, Simran Sangha and David Bekaert

Abstract

The goal of the project was to densify and extend the California archive of standardized interferogram products available through the JPL ARIA project, and to use these to extend our InSAR time series covering southern California beyond the 2019 Ridgecrest earthquake sequence (July 4-5, 2019). These products and time series are intended as contributions to the SCEC Community Geodetic Model (CGM). To facilitate the production of a combined CGM deformation product, we developed methods to align and reference these time series to GNSS displacement time series across the SCEC-defined region, and to estimate and remove coseismic offsets due to the Ridgecrest earthquakes, to allow the extension of our time series estimates beyond July 2019. We made additional contributions to the CGM by testing a bootstrapping approach for estimating errors in both our estimated velocities and those from the consensus CGM velocities. We have also started to analyze our velocity data to demonstrate its utility for studying fault creep.

Data and methodology

The state of California is covered by Sentinel-1 SAR data from 9 tracks (ascending and descending geometries; Figure 1). Sentinel-1 Geocoded UNWrapped (GUNW) interferograms are derived from this archive of SAR data by the Caltech-JPL Advanced Rapid Imaging and Analysis (ARIA) Center for Natural Hazards project (https://aria.jpl.nasa.gov/), and cover a period from the initial acquisitions to early 2022. GUNW interferograms, also known as 'Standard Displacement Products' (https://aria.jpl.nasa.gov/products/standard-displacement-products.html) are interferograms produced by the ARIA system–leveraging the ISCE processing software (Rosen et al., 2011)–to standard specifications (90 m resolution, unwrapped, supplied with interferometric correlation, SAR amplitude, line-of-sight and geocoding information). We build time-series composed of these interferograms (**Table 1**). This work represents an extension of ~3 years relative to the dataset we prepared under our previous proposed effort, which ended before the Ridgecrest earthquake sequence. Our goal with this project was to incorporate these products into work flows that can advance the SCEC Community Geodetic Model (CGM) project.

We performed a time-series analysis using the open source 'ARIA-tools' (Buzzanga et al., 2020) and 'MintPy' (Yunjun et al., 2019) packages to estimate average line-of-sight surface velocities from the ARIA GUNW interferograms, along with their corresponding uncertainties. ARIA-tools is a suite of tools that enables downloading, quality-checking, mosaicking, cropping and

masking of GUNW products in preparation for time series analysis. MintPy is a powerful time series analysis package that can produce Small BASeline subset (SBAS) solutions for deformation time series and deformation velocities from interferograms from a variety of packages. Combined, these two packages present a robust standard workflow for producing deformation products suitable for inclusion in the CGM.

As tropospheric water vapor remains the principal source of noise in InSAR data, we continue to leverage troposphere corrections derived from the GACOS project (Yu et al., 2018), based on the ECMWF HRES model, and evaluate velocities from the corrected data below (**Figure 1**). For tracks 64 and 71 where coseismic displacement was captured, a step function fit was added to account for the displacement field produced by the Ridgecrest earthquake sequence and more accurately constrain the secular velocity field. Velocity uncertainties are then estimated (**Figure 2**) by bootstrapping each InSAR time-series 1000 times and computing the standard deviation of the fit (Efron & Tibshirani, 1986). In each iteration observations are selected randomly to compute the fit, with the number of observations reflecting the original sample size of the dataset.

Table 1: Overview of Sentinel-1 data used in this project. ‘A’ or ‘D’ refer to ascending or descending acquisition geometries, respectively.

Track number and acquisition geometry	Observation start	Observation end	Number of acquisitions	Number of interferograms
42 D	2015/05/12	2022/01/23	158	427
115 D	2015/06/10	2022/01/16	152	341
144 D	2015/05/19	2021/08/03	125	320
173 D	2014/12/04	2022/01/20	217	590
35 A	2015/05/24	2022/01/23	191	333
71 D	2015/05/14	2022/01/25	200	483
137 A	2015/04/01	2022/01/18	216	473
166 A	2015/05/09	2021/12/21	105	281
64 A	2015/03/27	2022/01/25	199	425

Velocity results

We show results of our velocity analyses in **Figure 1**, with corresponding uncertainty estimates in **Figure 2**. Overall the features of the velocity estimates are consistent with expectations, even through the Ridgecrest earthquake sequence. The main pattern of velocities reverses in sign between ascending and descending tracks, consistent with a deformation field that is dominated by horizontal motions due to the San Andreas plate boundary fault system. The large negative

velocity feature seen in the central tracks (**Figure 1**), corresponding to the San Joaquin Valley, is consistent with rapid subsidence – most likely due to groundwater extraction. Coseismic signal associated with the M6.5 Monte Cristo Range, Nevada earthquake on May 15, 2020 is also captured in ascending track 64 (**Figure 1A**).

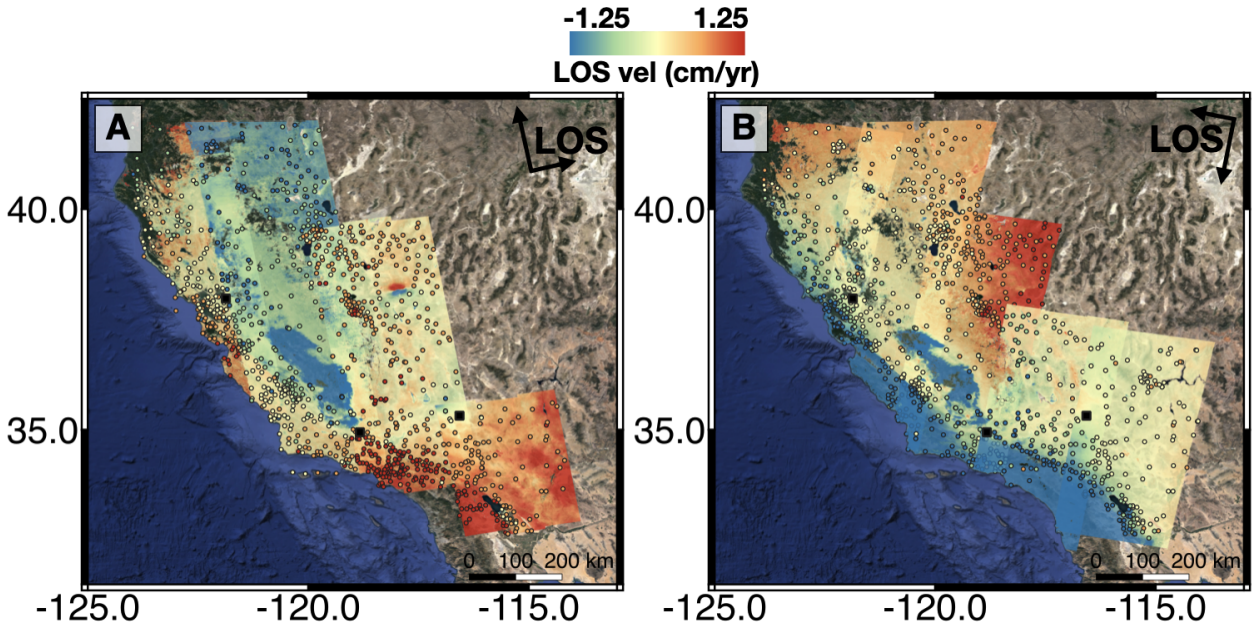

Figure 1: Line-of-sight surface velocities for ascending (A) and descending (B) passes after applying tropospheric corrections. Velocities are referenced to a single GNSS station (black square) for each track; GNSS stations used for velocity comparisons are also marked (colored dots). Positive motions indicate motion of the ground towards the satellite, and vice-versa.

Other contributions to the Community Geodetic Model

We have worked to characterize the uncertainties of the combined Community Geodetic Model product – which currently ends before the Ridgecrest earthquake sequence – by utilizing the same bootstrapping method we outlined above. The overall uncertainties, on the order of ~1 mm/yr, are low with respect to the geophysical signals in the data, though notably higher in the descending tracks (**Figure 3**). This is consistent with the difference in tropospheric activity between evening and morning acquisitions. In this case, this effect may be exacerbated as certain community contributions that have been incorporated into the combined model did not implement tropospheric corrections.

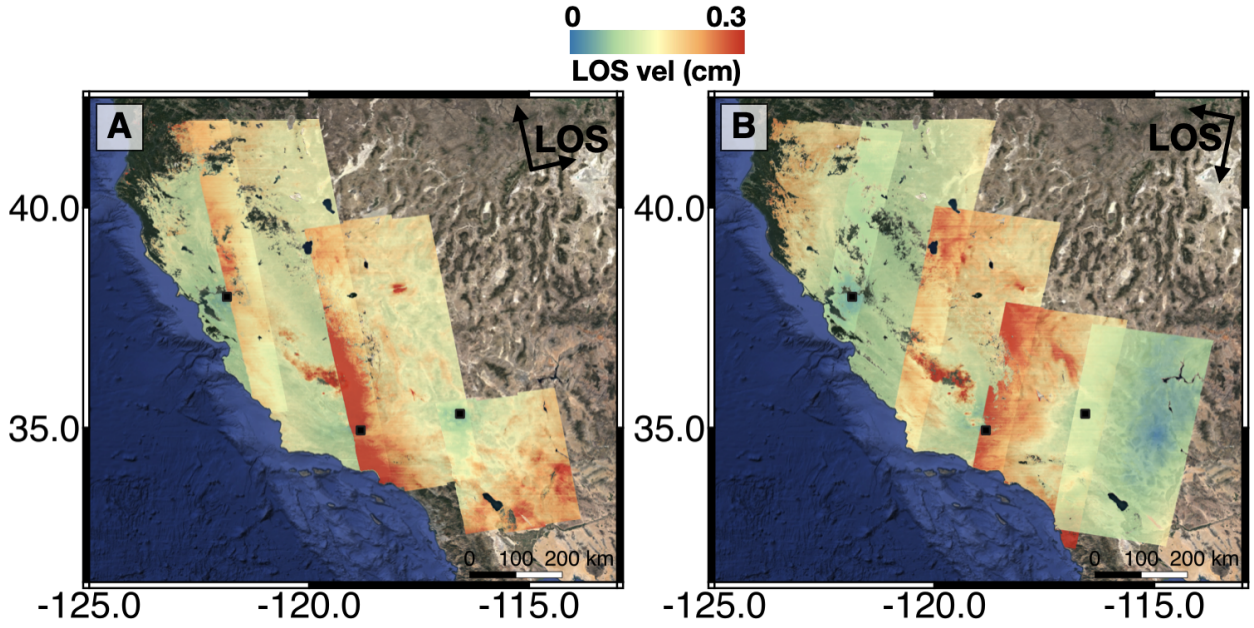

Figure 2: Uncertainties corresponding to ascending (A) and descending (B) pass LOS velocity fields from **Figure 1**, respectively. Refer to **Figure 1** for all other symbols and colors.

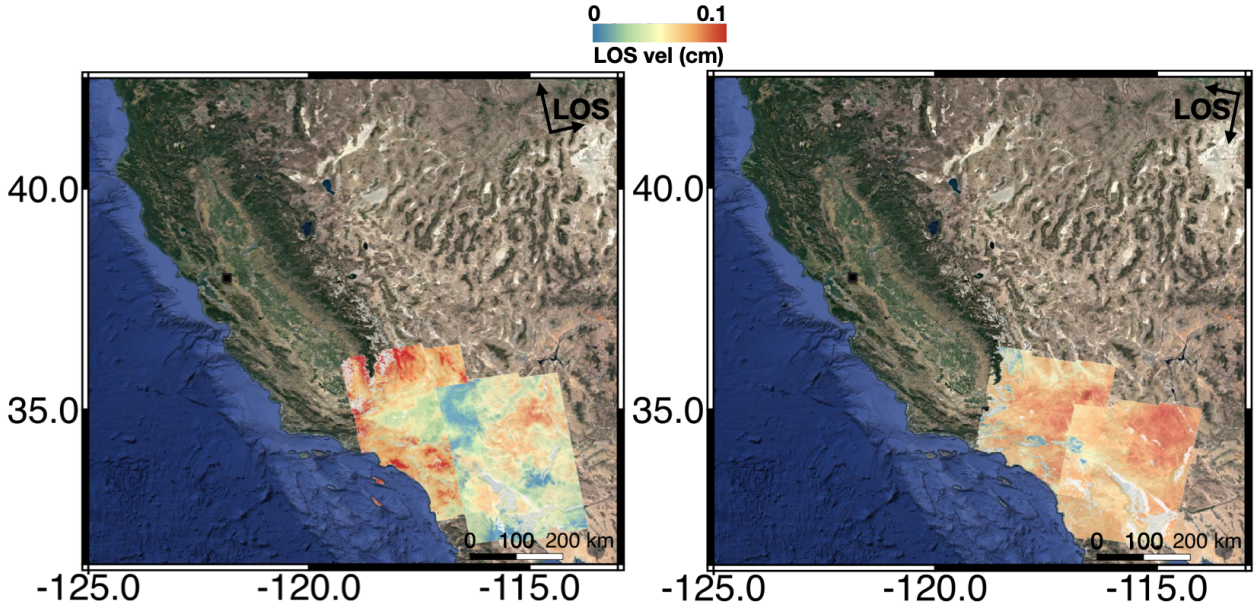

Figure 3: Uncertainties corresponding to ascending (A) and descending (B) pass LOS velocity fields from the combined Community Geodetic Model product (which spans up until the 2019 Ridgecrest earthquake sequence), respectively. Refer to **Figure 1** for all other symbols and colors.

Example application: fault creep detection

As part of our CGM-related work, we have been exploring the processed data to show its utility for studying geophysical processes of interest. A prescient application, for SCEC5 goals, is the detection of shallow aseismic slip ('fault creep') on the major active faults in southern California. The occurrence of creep on an active fault reduces the amount of strain that accumulates on it (e.g. Field et al., 2014), and in some frictional regimes may inhibit rupture propagation (e,g, Lozos et al., 2015), although this is still a matter of ongoing research (e.g. Harris et al., 2021). In addition to its role in modulating earthquake hazard, fault creep motivates fundamental scientific questions about the conditions (e.g. Bedrosian et al., 2004) and/or lithologies (e.g. Moore and Lockner, 2013) that may sustain it.

We apply the method of Jin and Funning (2017), previously used to detect creep along the northern Rodgers Creek fault in the San Francisco Bay Area, to our velocity field over central and southern California. We take regularly spaced (2 km spacing) cross-fault profiles, each 4 km long and centered on the fault, through one ascending and one descending InSAR data set, following the mapped Historic and Holocene fault surface traces from the USGS/CGS Quaternary Fault and Fold Database (USGS and CGS, 2006).

Our region-wide results are plotted in **Figure 4**. As expected, we resolve elevated right-lateral creep rates along the 'creeping segment' of the central San Andreas fault (up to ~28 mm/yr), and on its neighbor the Paicines fault (up to ~10 mm/yr). The majority of the other fault segments do not show evidence for significant creep, with the exception of the faults surrounding the Salton Sea – the Superstition Hills fault, the Imperial fault and the Coachella segment of the San Andreas fault – each of which shows creep up to ~5 mm/yr.

Summary and next steps

We have produced Sentinel-1 InSAR velocity maps covering the whole state of California using standard product interferograms from the ARIA project, using over 3500 interferograms from 9 tracks (**Table 1**). Our statewide analysis using standardized products allows us to capture earthquake-cycle processes e.g. (fault creep) and subsidence. The uncertainties derived from the combined community model (**Figure 3**) are notably smaller relative to the uncertainties for each of the tracks generated through our independent analysis (**Figure 2**). This discrepancy may be attributed to the fact that our independent analyses extend through the Ridgecrest earthquake sequence in 2019, such that derived velocity-fits are not an appropriate approximation of the changes reflected in post-seismic velocities. Thus, characterizing the post-seismic velocities separately may be warranted in tandem with other CGM efforts that work to extend their own time-series analysis.

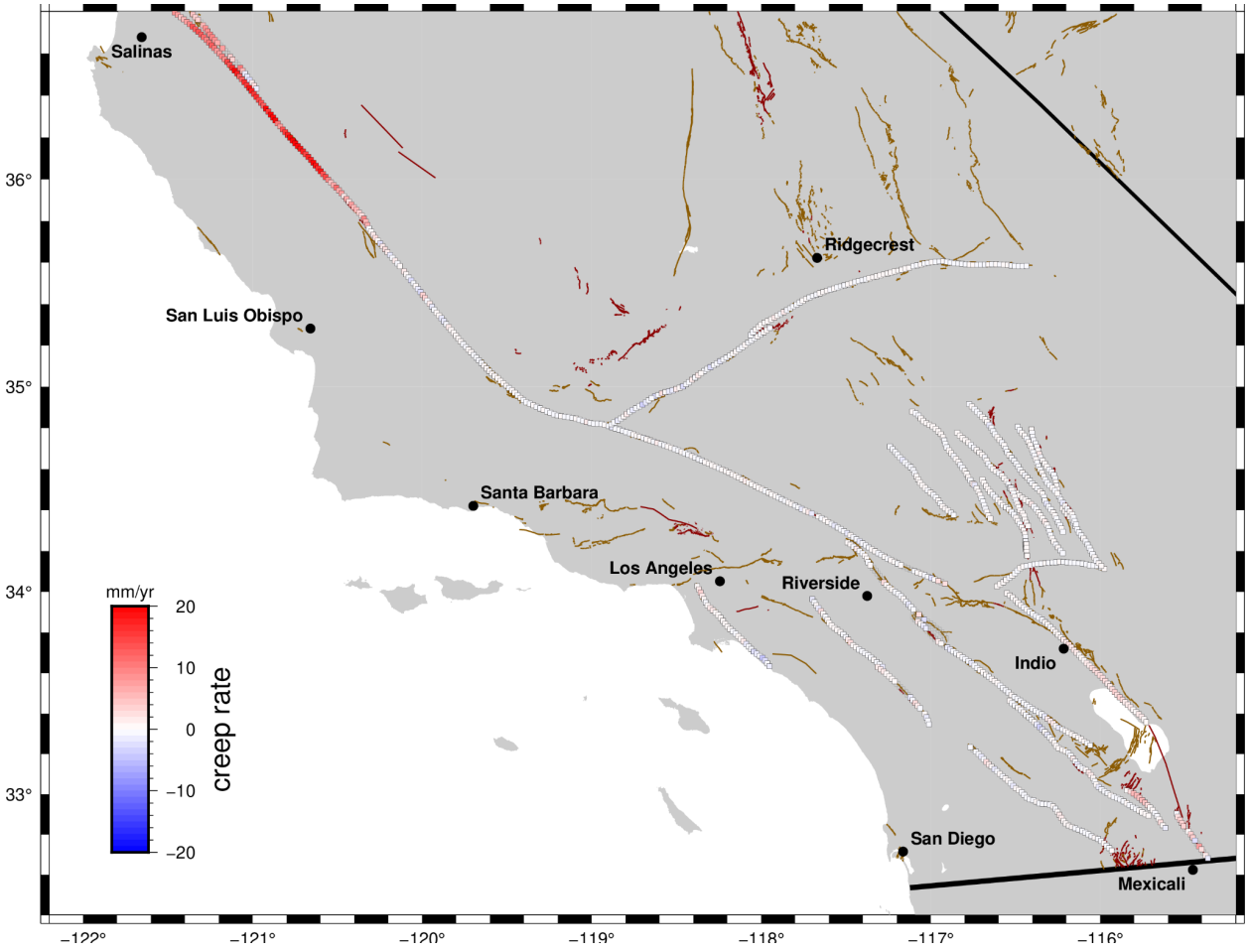

Figure 4: Distribution of shallow creep on faults of central and southern California, as estimated from inverting profile offsets from our California-wide velocity data set. Filled squares are locations where profile fits were successful; positive values (red colors) indicate right-lateral creep rates, negative values (blue) indicate left-lateral creep rates. Hollow squares indicate sites with vertical rates in excess of geologic observations. We identify creep on the central San Andreas, Paicines, Superstition Hills, Imperial and Coachella San Andreas faults.

References cited

Bedrosian, P. A., M. J. Unsworth, G. D. Egbert, and C. H. Thurber (2004), Geophysical images of the creeping segment of the San Andreas fault: Implications for the role of crustal fluids in the earthquake process, Tectonophysics, 385, 137– 158.

Buzzanga, B., Bekaert, D. P. S., Hamlington, B. D., and S. S Sangha (2020), Toward sustained monitoring of subsidence at the coast using InSAR and GPS: An application in Hampton Roads, Virginia. Geophys. Res. Lett., 47, e2020GL090013. https://doi.org/10.1029/2020GL090013

Efron, B., and R. Tibshirani (1986). Bootstrap methods for standard errors, confidence intervals, and other measures of statistical accuracy. Statistical science, 54-75.

Field, E. H., et al. (2014), Uniform California Earthquake Rupture Forecast, version 3 (UCERF3)—The time-independent model, Bull. Seismol. Soc. Am., 104, 1122– 1180.

Harris, R. A., Barall, M., Lockner, D. A., Moore, D. E., Ponce, D. A., Graymer, R. W., et al. (2021). A geology and geodesy based model of dynamic earthquake rupture on the Rodgers Creek-Hayward-Calaveras fault system, California. J. Geophys. Res. Solid Earth, 126, e2020JB020577. https://doi.org/10.1029/2020JB020577

Jin, L., and Funning, G. J. (2017), Testing the inference of creep on the northern Rodgers Creek fault, California, using ascending and descending persistent scatterer InSAR data, J. Geophys. Res. Solid Earth, 122, 2373– 2389, doi:10.1002/2016JB013535.

Lozos, J. C., R. A. Harris, J. R. Murray, and J. J. Lienkaemper (2015), Dynamic rupture models of earthquakes on the Bartlett Springs Fault, Northern California, Geophys. Res. Lett., 42, 4343– 4349, doi:10.1002/2015GL063802.

Moore, D. E., and D. A. Lockner (2013), Chemical controls on fault behavior: Weakening of serpentinite sheared against quartz-bearing rocks and its significance for fault creep in the San Andreas system, J. Geophys. Res. Solid Earth, 118, 1– 13, doi:10.1002/jgrb.50140

Rosen, P.A., Gurrola, E.M., Sacco, G. and H. Zebker (2011), InSAR Scientific Computing Environment (ISCE) – the home stretch, Abstract IN42A-02 presented at 2011 Fall Meeting. AGU, San Francisco, CA. p. 5.

U.S. Geological Survey, and California Geological Survey (2006), Quaternary fault and fold database for the United States. [Available at https://www.usgs.gov/programs/earthquake-hazards/faults, accessed March 14, 2022.]

Yunjun, Z., H. Fattahi and F. Amelung (2019), Small baseline InSAR time series analysis: Unwrapping error correction and noise reduction, Computers & Geosciences, 133, 104331, https://doi.org/10.1016/j.cageo.2019.104331

Yu, C., Li, Z., Penna, N. T., and P. Crippa (2018), Generic atmospheric correction model for interferometric synthetic aperture radar observations. J. Geophys. Res.: Solid Earth, 123, 9202– 9222. https://doi.org/10.1029/2017JB015305

Presentations

Sangha, S. S., Funning, G. J., and Bekaert, D. (2021, 08). The distribution of shallow creep on active faults in California, from a deformation velocity field derived from Sentinel-1 ARIA standard product interferograms. Poster Presentation at 2021 SCEC Annual Meeting.

Tymofyeyeva, E., Floyd, M., Bekaert, D., Funning, G. J., Guns, K. A., Liu, Z., Materna, K., Sandwell, D. T., Wang, K., and Xu, X. (2021, 08). Community Geodetic Model: Current status of the consensus InSAR model for deformation time series and velocities in Southern California. Poster Presentation at 2021 SCEC Annual Meeting.